AUT Journal of Modeling and Simulation

AUT J. Model. Simul., 58(2) (2026) 205-214
DOI: 10.22060/miscj.2026.26192.5514

# Design and Dosimetric Evaluation of a Range-Modulated Proton Therapy Nozzle for Ocular Melanoma Using GATE Monte Carlo

Zahra Mohammadi, Payvand Taherparvar *

Department of Physics, Faculty of Basic Sciences, University of Guilan, Rasht, Guilan.

**ABSTRACT:** Compared with conventional radiation techniques, proton therapy provides highly conformal dose distributions while reducing irradiation of surrounding normal tissues. Combining proton beams with different energies generates an extended Spread-Out Bragg Peak (SOBP) to cover the target. Passive scattering uses a range modulator wheel (RMW) to adjust proton energy and broaden the Bragg peak. In this study, a proton therapy nozzle comprising an RMW, compensator, and collimators was simulated for ocular tumor treatment using the GATE Monte Carlo code. A three-dimensional computational eye phantom including the lens, aqueous humor, cornea, choroid, retina, sclera, vitreous body, optic nerve, and tumor was developed to evaluate ocular dose distributions. The designed RMW generated a relatively uniform SOBP with a target length of 3.0 mm, a distal dose gradient (DDF) of 0.9 mm, and a d90 of 21.5 mm. The tumor dose was normalized to 100%, while relative doses were 52% for the lens, 63% for the aqueous humor, 62% for the cornea, 60% for the retina, 51% for the choroid, 44% for the sclera, 67% for the vitreous body, and 1% for the optic nerve. The results indicate that the RMW and compensator produced the intended SOBP and localized dose distribution within the modeled tumor geometry. These findings demonstrate the potential of the proposed nozzle configuration for achieving target-specific dose distributions while limiting irradiation of critical ocular structures. The developed computational framework provides a useful platform for investigating ocular proton-nozzle design and treatment-planning strategies.

**Review History:**

Received: Jul. 04, 2026
Revised: Sep. 11, 2026
Accepted: Sep.14, 2026
Available Online: Sep. 15, 2026

**Keywords:**

Proton Therapy
SOBP
RMW
GATE

## 1- Introduction

Uveal melanoma is the most common primary intraocular malignancy in adults and accounts for approximately 3–5% of all melanomas. Uveal melanomas can be classified according to tumor thickness as small (≤3 mm), medium (3–8 mm), and large (>8 mm) [1,2]. Treatment options include eye-preserving approaches such as radiotherapy, including brachytherapy and proton therapy, as well as laser-based procedures [3]. Proton therapy is used for selected uveal melanomas because of its favorable depth-dose characteristics and its ability to localize the dose within the target while limiting irradiation of surrounding ocular structures. In clinical proton therapy, a relative biological effectiveness (RBE) value of approximately 1.1 is commonly assumed relative to photon therapy; however, proton RBE may vary with linear energy transfer, dose, and the biological endpoint considered [4]. Therefore, accurate characterization of the physical dose distribution is important for the evaluation and optimization of ocular proton therapy.

The main approaches for proton beam delivery are active scanning and passive scattering [5]. In active scanning, magnetic fields are used to deflect a narrow proton beam in the lateral directions and to scan the target volume spot by spot [6,7]. Passive-scattering systems, in contrast, use mechanical beam-modifying components to broaden and shape the incident proton beam. A range modulator wheel (RMW) consisting of sectors with different thicknesses can generate proton beams with different residual ranges and thereby produce a Spread-Out Bragg Peak (SOBP) over the required target depth. Collimation components are used to define the lateral extent of the treatment field, while a compensator can modify the distal dose distribution according to the target geometry [8]. These components are particularly relevant to ocular proton therapy because ocular tumors are relatively small and are located in proximity to radiosensitive structures such as the lens, retina, optic nerve, and cornea.

Monte Carlo (MC) simulation is a well-established computational approach for modeling particle transport and particle–matter interactions in medical physics. Several MC codes, including MCNP, FLUKA, EGSnrc, Geant4, and GATE, have been developed and applied to radiation transport and dosimetry problems. GATE is built on the Geant4 simulation toolkit and provides a framework for defining particle sources, geometries, physics processes, and scoring quantities. These capabilities make GATE suitable

*Corresponding author's email: p.taherparvar@gmail.com

Copyrights for this article are retained by the author(s) with publishing rights granted to Amirkabir University Press. The content of this article is subject to the terms and conditions of the Creative Commons Attribution 4.0 International (CC-BY-NC 4.0) License. For more information, please visit https://www.creativecommons.org/licenses/by-nc/4.0/legalcode.



UNCORRECTED PROOF

for a wide range of applications in nuclear medicine and radiation therapy, including simulations in which absorbed dose and its spatial distribution are of primary interest [9,10].

Monte Carlo methods have been applied to ocular proton therapy for beamline characterization, proton range evaluation, and dose calculation in ocular tissues. Newhauser et al. [11] developed a Monte Carlo model of an ocular proton treatment beamline and compared the simulated beam characteristics with experimental measurements. Their results showed good agreement between simulation and measurement and demonstrated the feasibility of Monte Carlo-based modeling and virtual commissioning of ocular proton treatment beamlines. Grządziel et al. [12] subsequently compared Geant4 and MCNPX calculations of proton depth-dose distributions in water for ocular proton therapy. The small differences observed between the two codes highlighted the importance of code verification and comparison with reference or experimental data when Monte Carlo methods are used for proton dose calculations.

Other studies have investigated particle-therapy dose deposition and ocular modeling using different Monte Carlo approaches. Cheng et al. [13] investigated the dose distribution and irradiation-direction dependence of an 80 MeV/u carbon-ion beam in a computational model of the human eye using the FLUKA Monte Carlo code. Although their study focused on carbon-ion rather than proton therapy, it demonstrated the importance of beam incidence direction and ocular anatomy in determining the spatial distribution of radiation dose.

Rasouli et al. [14] developed a three-dimensional eye model incorporating the elemental composition of ocular tissues and compared proton dose deposition in the heterogeneous eye model with that in water and homogenized materials. Their results demonstrated that tissue composition and density can influence the calculated dose distribution and should therefore be considered when detailed ocular dose calculations are performed. Gul and Kuday [15] used GATE to develop a detailed geometrical model of the eye, including the eyeball, lens, lacrimal gland, optic nerve, optic chiasm, retina, tumor, cornea, and surrounding bone structures. They evaluated absorbed doses in ocular tissues using DoseActor and TLEDoseActor and investigated proton irradiation using multiple beam angles and energies. Their study primarily focused on treatment-planning considerations and dose evaluation for retinoblastoma rather than on detailed modeling and optimization of the proton treatment nozzle.

More recently, Piruzan et al. [16] developed a GATE-based model of a double-scattering proton treatment nozzle and investigated its dosimetric characteristics. Their work demonstrated the capability of GATE to model proton-nozzle components and evaluate the resulting beam properties. However, the double-scattering configuration differs from a passive-scattering system based on an RMW, in which the proton range is modulated through sectors of different thicknesses to generate an SOBP. Thus, detailed investigation of an integrated passive-scattering nozzle incorporating range modulation, beam collimation, and distal compensation remains relevant for ocular proton therapy.

In the present study, an integrated passive-scattering proton therapy nozzle was modeled using the GATE Monte Carlo framework for ocular tumor irradiation. The proposed nozzle incorporates a seven-sector range modulator wheel (RMW), a customized compensator, and collimation components. The RMW was designed to modulate the proton range and generate an SOBP suitable for the modeled ocular tumor, while the compensator was configured according to the tumor geometry to modify the distal dose distribution. A three-dimensional computational eye phantom comprising the lens, aqueous humor, cornea, choroid, retina, sclera, vitreous body, optic nerve, and a modeled ocular tumor was subsequently developed to evaluate dose deposition in the tumor and surrounding ocular structures. The resulting proton range, SOBP characteristics, distal dose fall-off, and absorbed dose distributions were evaluated to characterize the dosimetric performance of the proposed configuration.

## 2- Model and Simulation

Initially, to benchmark the proton transport and range calculations of the simulation model, a water-phantom configuration based on the beam-transport conditions reported in a previous study [17] was considered. Nine proton energies, namely 75, 100, 120, 140, 160, 180, 200, 225, and 250 MeV, were investigated. Consistent with the model described in reference [17], the proton source was defined as a disk with a radius of 10 cm located in the plane at $z = -300$ cm, with the proton trajectories directed along the z-axis. A water phantom with dimensions of $40 \times 80 \times 80$ cm³ was employed to ensure that the protons did not escape through the phantom boundaries. The proton ranges obtained from the present GATE simulations were subsequently compared with the corresponding NIST PSTAR reference values, as summarized in Table 1. The calculated ranges were also compared with the corresponding CSDA values [18]. The relative differences between the GATE-derived and NIST ranges were approximately 2.2–5.2%, whereas those between the CSDA and NIST values were approximately 0.2–3.5%. These results indicate reasonable agreement between the present GATE calculations and the established NIST PSTAR and CSDA reference data.

GATE 9.2 was used to simulate proton transport through the treatment nozzle and the ocular phantom. An initial proton energy of 75 MeV was selected to provide a proton range compatible with the modeled ocular anatomy and tumor depth after passage through the beam-modifying components. The incident beam was subsequently characterized in a water phantom, and composite foils consisting of lead and Lexan with varying thicknesses were placed in the proton beam path to generate range-shifted Bragg peaks. Using GATE's specialized scoring actor, the resulting Bragg peaks from energy deposition in the phantom were recorded and subsequently analyzed in MATLAB. The range-shifted Bragg peaks were selected to span the depth range corresponding to the intended SOBP region in the ocular phantom. Subsequently, the relative intensity weightings required to produce a uniform dose distribution across the SOBP region

UNCORRECTED PROOF

**Table 1. Comparison of proton ranges obtained from GATE simulations with NIST and CSDA ranges in a homogeneous water phantom [18].**

| Energy(MeV) | GATE(cm) | NIST(cm) | CSDA(cm) | Relative difference, (%) GATE vs NIST | Relative difference, (%) CSDA vs NIST |
|---|---|---|---|---|---|
| 75 | 4.5 | 4.6 | 4.7 | 2.17 | 2.17 |
| 100 | 7.3 | 7.707 | 7.5 | 5.2 | 2.6 |
| 120 | 10.2 | 10.65 | 10.5 | 4.2 | 1.4 |
| 140 | 13.4 | 13.96 | 14 | 4.01 | 0.2 |
| 160 | 17 | 17.63 | 17.5 | 3.57 | 0.7 |
| 180 | 20.9 | 21.63 | 21.5 | 3.37 | 0.6 |
| 200 | 25.1 | 25.93 | 25 | 3.2 | 3.5 |
| 225 | 30.8 | 31.71 | 31 | 2.86 | 2.2 |
| 250 | 36.9 | 37.90 | 37.5 | 2.63 | 1.0 |

at position x were calculated using the following relationship:

$$D = \sum_i w_i D_i(x) \quad (1)$$

where D is the target total dose within the Spread-Out Bragg Peak (SOBP) region, i is the index representing each proton beam (in this study, i = 1 to 7, corresponding to the seven sectors of the RMW), $w_i$ is the relative intensity weighting (or contribution fraction) of the i-th proton beam, which is the unknown quantity to be determined, and $D_i(x)$ is the physical dose deposited by the i-th proton beam at position x along the beam axis (depth), obtained from the GATE Monte Carlo simulation. To solve for the weightings $w_i$, we construct a dose matrix D whose elements $D_{m,n}$ represent the dose contribution from the n-th proton beam at the m-th sampling point along the SOBP region. The optimization problem is then solved using the following matrix equation:

$$w_n = D \sum_m ((D^T)^{-1})_{m,n} \quad (2)$$

where $w_n$ is the relative intensity weighting of the n-th proton beam, D is the transport matrix, with elements $D_{m,n}$ representing the dose deposited by the n-th beam at the m-th depth position, m is the index of the sampling points along the depth (these points are selected within the SOBP region to ensure uniform dose coverage), n is the index of the proton beams (from 1 to 7, corresponding to the seven RMW sectors), $D^T$ is the transpose of the transport matrix D, and $(D^T)^{-1}$ is the inverse of the transposed matrix. By calculating $w_i$, the angle of each sector can be estimated using the relationship $w_i * 360^o$. Since each sector's arc length directly corresponds to the relative intensity contribution of its associated beam to the SOBP dose distribution, optimization of these parameters is critical for enhancing nozzle performance [19]. To generalize the results for ocular tumor treatment planning, a comprehensive simulation of the proton therapy nozzle was performed. While longitudinal dose modulation was achieved using a range modulation wheel, this approach alone proved insufficient for covering tumors with irregular longitudinal profiles. To address this limitation, a PMMA compensator was incorporated alongside the modulation wheel to precisely match the energy deposition to the tumor's spatial distribution and curvature. Additionally, collimators were modelled to minimize beam scattering. Figure 1 illustrates the complete nozzle geometry and the designed phantom within the GATE simulation environment. The specifications of all nozzle components, including materials and dimensions, are detailed in Tables 2 and 3

The simulated proton therapy nozzle geometry in the GATE consists of RMW, collimators, and a compensator. The RMW is a pivotal component in passive scattering proton therapy systems. Its primary function is to transform a narrow, monoenergetic Bragg peak into a Spread-Out Bragg Peak (SOBP), thereby ensuring a uniform therapeutic dose distribution across the entire depth of the target tumor [21]. The RMW consists of a rotating wheel featuring steps of varying thicknesses along its circumference. Protons traversing thinner steps undergo less energy attenuation, allowing them to penetrate to greater tissue depths, whereas thicker steps absorb more energy, causing protons to stop at shallower depths. As the wheel rotates continuously, successive steps are rapidly placed in the beam's path. The resulting individual Bragg peaks at different depths are superimposed over time, summing to produce the final SOBP. The rotation period of the range modulation wheel is designed to be substantially shorter than the total irradiation time, allowing the modulation effects associated with the individual wheel sectors to be effectively averaged over the treatment period. In addition, the beam current is synchronously modulated with the rotation of the range modulation wheel according to the thickness of the

UNCORRECTED PROOF

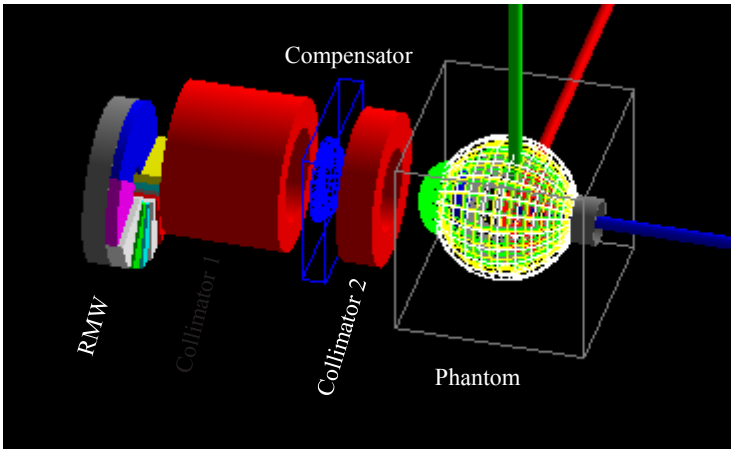



**Fig. 1. A view of the proton therapy nozzle geometry in the GATE environment.**

**Table 2. Components designed in the proton therapy nozzle.**

| Nozzle components | Material | Inner radius (mm) | Length (mm) | Outer radius (mm) |
|---|---|---|---|---|
| Collimator 1 | Brass | 7 | 6 | **13** |
| Collimator 2 | Brass | 8 | 20 | **13** |
| Compensator | PMMA | 0 | 4 | **7** |
| Range Modulation Wheel | Lead and Lexan | 1 | 11 | **100** |

**Table 3. Materials used in proton therapy nozzle.**

| Material | Composition | density (g/cm3) |
|---|---|---|
| Lead | Pb (100%) | 11.35 |
| Lexan | H (5.5%): C (75.6%): O (18.9%) | 1.2 |
| Brass | Cu (67%): Zn (33%) | 8.35 |
| PMMA | H (8%): C (60%): O (32%) | 1.195 |
| Water | $H_2O$ | 1.0 |
| Air | N (75.6%): O (23.1%): Ar (1.3%) | 0.001225 |

UNCORRECTED PROOF

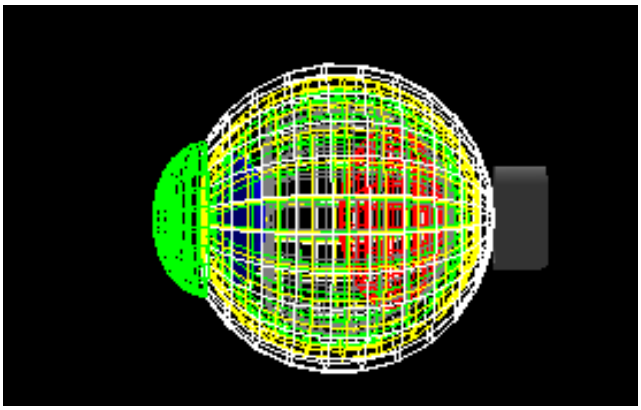


**Fig. 2. A view of the simulated eye phantom in the GATE environment.**

instantaneous wheel sector, thereby controlling the relative contribution of each proton range and producing a uniform dose distribution [21]. Although the exact rotation speed is not a fixed universal value and depends on the specific system design, a key advantage of the RMW is its ability to achieve nearly instantaneous range shifts, in contrast to systems that require several seconds to alter accelerator energy. It should be noted, however, that this approach linearly increases the overall beam-on time. From a relative temporal perspective, energy switching times in modern Pencil Beam Scanning (PBS) systems typically range from fractions of a second to a few seconds. Nevertheless, precise rotation timing parameters must always be obtained from the technical specifications of the specific device in use. When a sector is rotated into the proton beam path, it generates a distinct Bragg peak at a specific depth. As a critical component of the nozzle assembly, the RMW enables longitudinal dose modulation. Within the simulation environment, two cylindrical brass collimators were positioned along the beam path. As shown in Figure 1, these collimators serve to shape the beam profile by reducing lateral scattering and minimizing off-axis dose deposition. Their strategic placement helps reduce scattered radiation within the treatment system. A compensator is a customized device used to shape the proton beam and deliver radiation more precisely to the target. Compensators are typically made from materials such as acrylic or wax and are designed with specific thicknesses and shapes. The primary purpose of a compensator is to conform the dose distribution to the distal surface of the target (tumor), thereby helping to maximize dose delivery to the tumor while minimizing the dose to healthy tissue beyond the target [22].

To achieve a realistic simulation of dose deposition in the eye, a relatively detailed eye phantom was defined in the GATE code, as shown in Figure 2. The phantom consisted of the lens, aqueous humor, cornea, choroid, retina, sclera, vitreous body, optic nerve, and tumor. The elemental weight fractions and densities of the different ocular components are listed in Table 4. The sclera, choroid, retina, and vitreous body were modeled as concentric spheres with radii of 12, 11, 10, and 9 mm, respectively. The cornea was modeled as an elliptical shell bounded by two concentric ellipses and the outer spherical surface of the sclera. The aqueous humor of the anterior chamber was modeled as the volume bounded anteriorly by the posterior surface of the cornea and posteriorly by the anterior surface of the lens. The optic nerve was modeled as a 4-mm-long cylinder positioned at the posterior region of the eye, while the lens was modeled as an ellipsoidal structure with a thickness of 10 mm. The tumor was modeled as an elliptical shape with a thickness of 8 mm, positioned at the posterior pole of the eye (choroid region). This geometry was selected based on the clinical classification of uveal melanoma, which categorizes tumors according to thickness: small (≤3 mm), medium (3–8 mm), and large (>8 mm). The 8-mm tumor thickness represents the upper limit of the medium-thickness category, which is among the most challenging cases for proton therapy and is therefore of significant clinical relevance. The elliptical (dome-shaped) morphology approximates the typical presentation of choroidal melanomas, which are commonly described as nodular or dome-shaped lesions. While this represents an idealized tumor model, it is clinically motivated and allows for systematic evaluation of the treatment planning parameters, including the design of the range modulation wheel and compensator. The QGSP_BIC_HP_EMY physics list was used to model the relevant electromagnetic and hadronic interactions of the transported particles. A production cut of 0.1 mm was applied for gamma rays, electrons, and positrons across all regions (World, Phantom, and Tumor), while a range cut of 0.1 mm was used for protons. A total of 10□ primary protons were simulated to achieve a statistical uncertainty of less than 3%. The proton beam was defined using the General Particle Source (GPS) command as a monoenergetic 75 MeV beam with no energy spread, a uniform circular spatial distribution, and a radius of 7 mm. The beam was directed along the positive z-axis, perpendicular to the phantom surface, with a source-to-phantom distance of 150 mm. A 3D DoseActor was defined with voxel dimensions of 0.1 × 0.1 × 0.1 $mm^3$. The absorbed dose in all eye tissues was scored

UNCORRECTED PROOF

**Table 4. Weight fraction and density of elements that make up different components of the eye [20].**

| | sclera | choroid | Retina | vitreous | optic nerve | Lens | the cornea | Tumor |
|---|---|---|---|---|---|---|---|---|
| H | 9.6 | 9.4 | 9.4 | 11.0867 | 10.70 | 9.60 | 10.16 | 10.08 |
| C | 9.90 | 21.20 | 21.20 | 0.068 | 9.5 | 19.50 | 11.99 | 4.10 |
| N | 2.20 | 5.60 | 5.60 | _ | 0.20 | 5.70 | 3.64 | 1.10 |
| O | 74.40 | 61.50 | 61.50 | 88.052 | 76.70 | 64.60 | 74.11 | 83.2 |
| Na | _ | 0.25 | 0.25 | 0.2645 | 0.20 | 0.10 | _ | _ |
| Mg | 0.50 | _ | _ | 0.0025 | _ | _ | _ | 0.30 |
| Cl | 0.30 | 0.39 | 0.39 | 0.502 | 0.30 | 0.10 | _ | 0.40 |
| P | 2.20 | 0.51 | 0.51 | 0.002 | 0.30 | 0.10 | _ | _ |
| S | 0.90 | 0.64 | 0.64 | _ | 0.20 | 0.30 | 0.09 | 0.10 |
| K | _ | 0.51 | 0.51 | 0.0171 | 0.30 | _ | _ | _ |
| Ca | _ | _ | _ | 0.005 | _ | _ | _ | _ |
| (g/cm³) density | 1.09 | 1.04 | 1.04 | 1.00 | 1.039 | 1.07 | 1.05 | 1.03 |

using the DoseActor in GATE. The DoseActor automatically calculates the relative statistical uncertainty for each voxel based on the standard error of the mean dose. The uncertainty values reported in this study are those directly provided by the GATE DoseActor output.

## 3- Results and Discussion

Figures 3a and b illustrate the normalized dose profile curves generated by the interaction of a 75 MeV proton beam with the water phantom and the ocular phantom. Each normalized dose curve corresponds to one of the seven steps of the RMW employed to produce a SOBP. The dose data from each step were weighted according to their respective contributions to the SOBP formation, based on Equations 1 and 2. Subsequently, the angular dimensions of each sector within the modulation wheel were derived, thereby enabling the design of an optimized wheel configuration. An optimized wheel design ensures uniform dose distribution within the tumor area, minimizes beam scattering to healthy tissues, and improves treatment efficiency. The results of the SOBP region generated by the designed wheel in the eye phantom are presented in Figure 4.

The characteristics of the generated SOBP can be evaluated using parameters recommended by the International Commission on Radiation Units and Measurements (ICRU). These parameters, outlined in Table 5, include the depth of penetration, the distal dose fall-off (DDF), the SOBP length, and the target length. The depth of penetration (d90) is defined as the distance along the beam axis at which the dose reaches 90% of its maximum value near the distal edge of the beam. The distal dose fall-off (DDF) represents the spatial interval over which the dose decreases from 80% to 20% of the maximum along the beam path. The SOBP length (m90) corresponds to the distance between the points at which the dose reaches 90% of the maximum at the proximal and distal ends of the SOBP. The target length (treatment length) is defined as the distance from the proximal edge, corresponding to the 90% dose level, extended by twice the DDF measured from the 50% dose level at the distal edge of the beam. The results presented in Table 5 indicate that the selected RMW sector thicknesses were suitable for generating the desired dose distribution over the tumor region. For the modeled RMW, seven Lexan sectors with thicknesses ranging from 1 to 7 mm were attached to a cylindrical lead component with a diameter of 10 cm and a thickness of 9 mm. The corresponding arc angles of the seven sectors were 121.5°, 103.4°, 35.9°, 28.1°, 19.5°, 18.9°, and 32.7°, respectively. These arc angles were determined using Equation (2) from the relative dose contributions required at different depths, as derived from the Bragg curve of the incident proton beam shown in Figure 3. Accordingly, the sector angles were selected to provide the appropriate weighting of the individual range-shifted Bragg peaks and generate the desired spread-out Bragg peak (SOBP) across the tumor region.

After generating a relatively uniform SOBP over the selected target region and designing the compensator according to the tumor geometry, the absorbed dose was calculated for all modeled ocular structures. Table 6 presents the calculated relative absorbed doses. The absorbed dose in the tumor was used as the normalization reference

UNCORRECTED PROOF

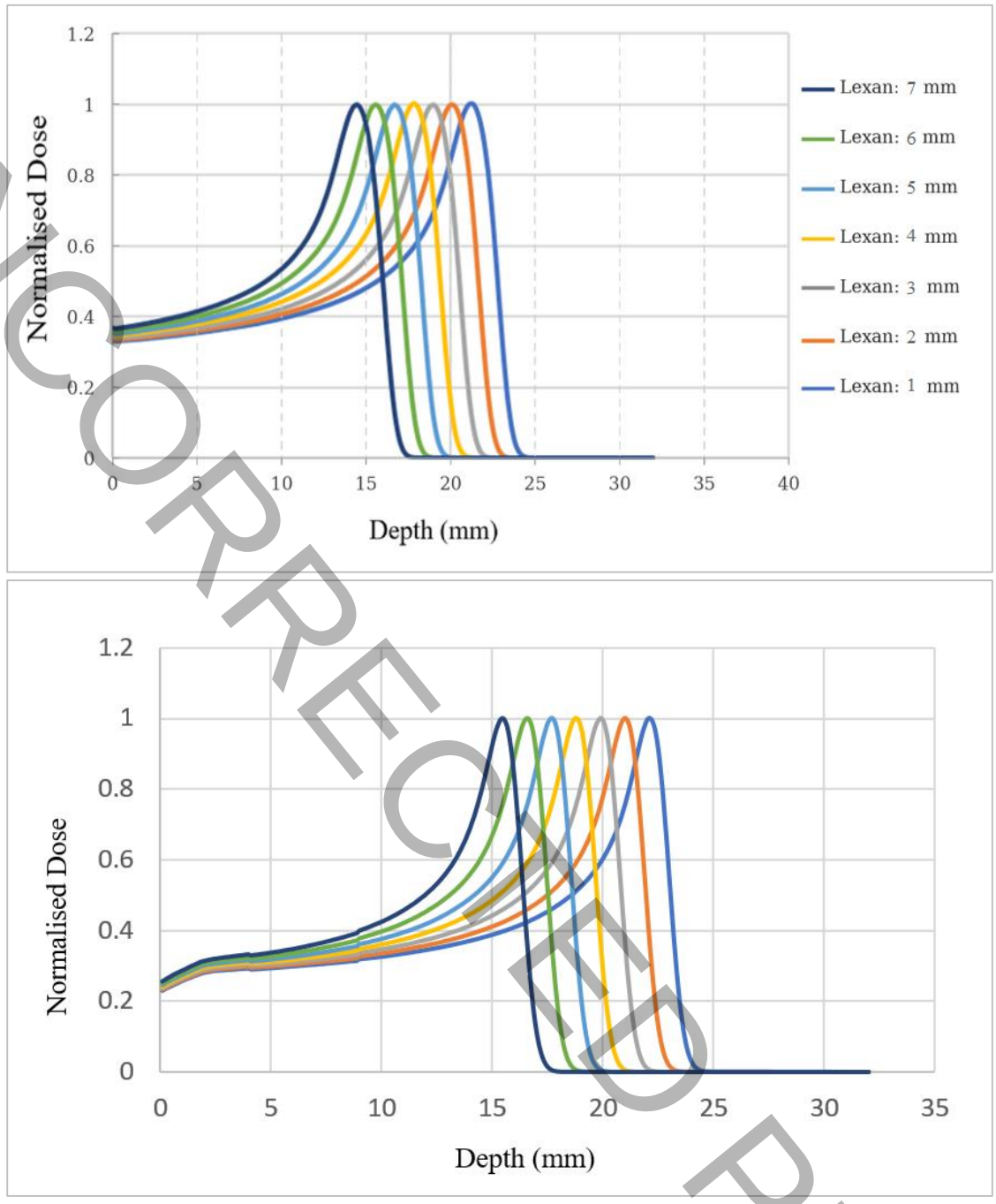



**Fig. 3. Dose profile curves for proton beams impinging on (a) the water phantom and (b) the eye phantom.**

(100%), and the absorbed doses in all ocular structures were expressed relative to the tumor dose. Among the evaluated structures, the optic nerve received the lowest relative dose (1%), whereas the vitreous body, aqueous humor, and cornea received relatively higher doses. The relatively higher doses in the aqueous humor and cornea are consistent with their anatomical location along or near the incident proton-beam path. Overall, the calculated dose distribution reflects the dependence of ocular dose deposition on beam trajectory and the anatomical position of the individual ocular structures.

For the visual analysis of the results, a two-dimensional energy deposition image is shown in Figure 5. The image was extracted in MHD format from the GATE simulation and imported into MATLAB. In the two-dimensional energy deposition image, the colors represent different levels of deposited energy at various spatial locations within the volume. The red regions indicate areas of relatively high radiation dose, corresponding primarily to the tumor, whereas

UNCORRECTED PROOF

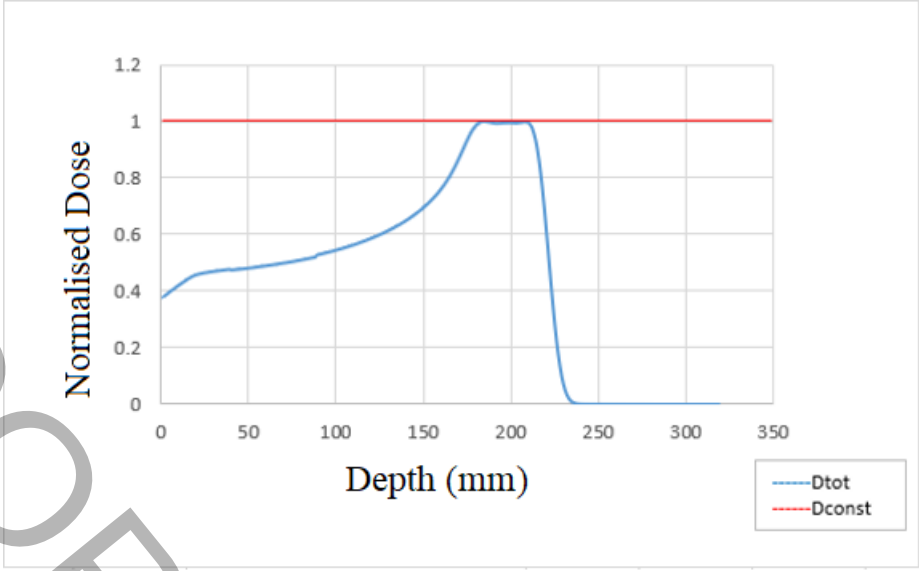



**Fig. 4. SOBP diagram resulting from RMW designed in proton therapy nozzle in eye phantom.**

**Table 5. Calculated parameters characterizing the SOBP generated by the designed RMW in the eye phantom.**

| The parameters of the beam evaluation | Eye Phantom (mm) |
|---|---|
| d90 | **21.5** |
| DDF | **0.9** |
| m90 | **2.7** |
| Target length | **3** |

**Table 6. Relative absorbed dose in the modeled ocular structures.**

| eye tissue | Percentage |
|---|---|
| Tumor | 100 |
| Lens | 52 |
| optic nerve | 1 |
| Aqueous | 63 |
| Choroid | 51 |
| Retina | 60 |
| Cornea | 62 |
| Vitreous | 67 |
| Sclera | 44 |

Note: The statistical uncertainty of the Monte Carlo dose calculations was less than 3% for all scored regions

the blue regions represent healthy tissues receiving relatively low doses. The image clearly demonstrates a higher dose concentration within the tumor region compared with the surrounding anterior and posterior regions. Furthermore, a relatively uniform dose distribution is observed within the tumor itself.

## 4- Conclusions

In this study, a passive-scattering proton therapy nozzle for ocular tumor irradiation was modeled using the GATE Monte Carlo toolkit. An optimized seven-sector RMW configuration was developed to generate an SOBP suitable for the modeled tumor geometry, while a compensator was incorporated to conform the distal dose distribution to the tumor shape. The resulting SOBP had a target length of 8 mm, a distal dose fall-off of 0.9 mm, and a penetration depth (d□□) of 21.5 mm. The tumor dose was used as the normalization reference (100%), and the relative absorbed doses in the surrounding ocular structures were lower, with values ranging from 1% in the optic nerve to 67% in the vitreous body. These results indicate the feasibility of using an integrated GATE model to investigate RMW-based passive-scattering nozzle configurations and their associated ocular dose distributions. However, the present results are based on an idealized eye and tumor geometry and have not been experimentally validated. Further experimental studies using

UNCORRECTED PROOF

anthropomorphic or tissue-equivalent phantoms are therefore required to assess the dosimetric performance of the proposed nozzle under realistic treatment conditions.

## References


[1] Krantz BA, Dave N, Komatsubara KM, Marr BP, Carvajal RD. Uveal melanoma: epidemiology, etiology, and treatment of primary disease. Clin Ophthalmol. 2017;11:279–289.

[2] Brewington BY, Shao YF, Davidorf FH, Cebulla CM. Brachytherapy for patients with uveal melanoma: historical perspectives and future treatment directions. Clin Ophthalmol. 2018;12:925–934.

[3] Taherparvar P, Fardi Z. Development of GATE Monte Carlo code for simulation and dosimetry of new I-125 seeds in eye plaque brachytherapy. Nucl Med Mol Imaging. 2021;55(2):86–95.

[4] Taghipour H, Taherparvar P. Development of modified microdosimetric kinetic model for relative biological effectiveness in proton therapy. Radiat Environ Biophys. 2022;61(3):375–390.

[5] Kooy HM, Clasie BM, Lu HM, et al. A case study in proton pencil-beam scanning delivery. Int J Radiat Oncol Biol Phys. 2010;76:624.

[6] Furukawa T, et al. Performance of the NIRS fast scanning system for heavy-ion radiotherapy. Med Phys. 2010;37(11):5672–5682.

[7] Nomura K, et al. Biological effects of passive scattering and spot scanning proton beams at the distal end of the spread-out Bragg peak in single cells and multicell spheroids. Int J Radiat Biol. 2021;97(5):695–703.

[8] Michaelidesová A, et al. In vitro comparison of passive and active clinical proton beams. Int J Mol Sci. 2020;21(16).

[9] Paganetti H, et al. Clinical implementation of full Monte Carlo dose calculation in proton beam therapy. Phys Med Biol. 2008;53:4825–4853.

[10] Grevillot L, et al. Optimization of GEANT4 settings for proton pencil beam scanning simulations using GATE. Nucl Instrum Methods Phys Res B. 2010;268:3295–3305.

[11] Newhauser W, Koch N, Hummel S, Ziegler M, Titt U. Monte Carlo simulations of a nozzle for the treatment of ocular tumours with high-energy proton beams. Phys Med Biol. 2005;50:5229–5249.

[12] Grządziel M, Konefał A, Zipper W, Pietrzak R, Bzymek E. Verification of the use of GEANT4 and MCNPX Monte Carlo codes for calculations of the depth-dose distributions in water for the proton therapy of eye tumours. Nukleonika. 2014;59(2):61–66.

[13] Cheng-Guo P, You-Wu S, Wen-Jun W, Xiao-Ming L, Jun-Kui X, Wu-Yuan L, Jiao Y, Ze-En Y. Monte Carlo simulation of carbon ion radiotherapy for the human eye. Chin Phys C. 2015;39(1):018201.

[14] Rasouli SF, Masoudi SF, Keshazare S, Jette D. Effect of elemental compositions on Monte Carlo dose calculations in proton therapy of eye tumors. Radiat Phys Chem. 2015; 117, 112-119.

[15] Gul I, Kuday S. Retinoblastoma radiotherapy treatment optimizations through GATE simulations. Cumhuriyet Sci J. 2022;43(4):708–715.

[16] Piruzan E, Vosoughi N, Mahani H. A comprehensive GATE Monte Carlo model for a double scattering proton treatment nozzle. J Nucl Sci Technol. 2022;99(2) .

[17] Zheng Y, Fontenot J, Taddei P, Mirkovic D, Newhauser W. Monte Carlo simulations of neutron spectral fluence, radiation weighting factor and ambient dose equivalent for a passively scattered proton therapy unit. Phys Med Biol. 2008;53:187–201.

[18] Berger MJ, Coursey JS, Zucker MA, Chang J. ESTAR, PSTAR, and ASTAR: computer programs for calculating stopping-power and range tables for electrons, protons, and helium ions, version 1.2.3. Gaithersburg, MD: National Institute of Standards and Technology; 2005. Available from: NIST Standard Reference Database 124.

[19] Paganetti H. Proton Therapy Physics. Boca Raton, FL: CRC Press; 2011. p. 18–57.

[20] Asadi S, Vaez-zadeh M, Masoudi SF, Rahmani F, Knaup C, Meigooni AS. Gold nanoparticle-based brachytherapy enhancement in choroidal melanoma using a full Monte Carlo model of the human eye. J Appl Clin Med Phys. 2015;16(5):344–357.

[21] Sánchez-Parcerisa D, Kirk M, Fager M, Burgdorf B, St James S, Shih H, Kooy HM. Fast range switching of passively scattered proton beams using a modulation wheel and dynamic beam current modulation. Phys Med Biol. 2014;59(7):N19–N26.

[22] Kang M, Wei S, Choi J, Lin H. A universal range shifter and range compensator can enable proton pencil beam scanning single-energy Bragg peak FLASH-RT treatment using current commercially available proton systems. Int J Radiat Oncol Biol Phys. 2022;112(3):3–4.


UNCORRECTED PROOF

UNCORRECTED PROOF

**HOW TO CITE THIS ARTICLE**
*Z. Mohammadi, P. Taherparvar, Design and Dosimetric Evaluation of a Range-Modulated Proton Therapy Nozzle for Ocular Melanoma Using GATE Monte Carlo, AUT J. Model. Simul., 58(2) (2026) 179-188.*

**DOI:** 10.22060/miscj.2026.26192.5514